International Journal of Nanoscience
Vol. 10, No. 3 (2011) 479–486

DOI: 10.1142/S0219581X11008241

World Scientific
www.worldscientific.com

LOW TEMPERATURE SYNTHESIS AND ELECTRONIC PROPERTIES OF NTC TEMPERATURE SENSOR SPINEL-TYPE OXIDES NANOPOWDERS

S. M. HOSSEINI*, B. GHANBARI SHOHANY,
N. AZAD and A. KOMPANY
Department of Physics
Materials and Electroceramics Laboratory
Ferdowsi University of Mashhad
Mashhad, Iran
**sma_hosseini@yahoo.com*

Received 26 July 2010
Accepted 5 November 2010

$NiCo_xMn_{2-x}O_4$ ($x = 0.4, 0.8, 1.2, 1.6$) thermistor with nanopowders have been synthesized by the auto-combustion method at low temperatures. The size and morphology of the calcinated powders have been investigated using XRD and TEM techniques. The average particle size was estimated to be about 65 nm in diameter with the cubic and cubic + tetragonal phases for low and high cobalt concentrations, respectively. The grain size of NTC ceramics sintered at 1200°C is verified with scanning electron microscopy (SEM) images. Upon increasing the cobalt concentration, the grain size of NTC samples increases from about 2 μm to a few μm in size.

The formation of spinel structure of powders has been studied by Fourier transform infrared (FTIR) spectroscopy. An *ab initio* calculation of electronic properties of $NiCo_{0.8}Mn_{1.2}O_4$ using full potential of the linear augmented plane wave (FP-LAPW) method has been performed. The results indicate that only the 3*d*-Mn orbitals play an important role in the conduction mechanism. The dependency of material resistivity constant (B) and temperature coefficient (α) have been measured.

Keywords: Sol–gel processes; electrical conductivity; spinels; thermistors.

1. Introduction

Spinel materials based on transition metals such as Ni, Co, and Mn are widely used as negative temperature coefficient (NTC) thermistors,[1] which are employed in the manufacturing of temperature measurement devices such as sensors. NTC thermistors have spinel structure with general formula AB_2O_4, where A and B are related to tetrahedral and octahedral lattice sites, respectively.[2]

The electrical conductivity of materials with spinel structure has been explained via electron conduction on a small polaron hopping process.[3] As temperature increases, the electron moves from site to site by thermally activated hopping. At low

*Corresponding author.

temperatures, the electron tunnels slowly through the crystal. In spinel structure, the transfer of electrical charges occurs by the hopping movement of electrons between the $3d$-B^{+3} and $3d$-B^{+4} orbitals present at the octahedral sites in the lattice. The electrical conductivity of Mn_3O_4 and similar spinel structures, with Mn^{+2} on tetrahedral sites and Mn^{+3} on octahedral sites, is not very significant. This structure does not contain ions of the same element but with different charges on similar sites, as required for electron hopping. However, the substitution of Ni or Co for Mn shifts Mn_3O_4 from an insulator to a semiconductor increasing the conductivity. Ni^{+2} occupies octahedral sites and the charge balance is maintained by the conversion of Mn^{+3} to Mn^{+4}, thus providing a basis for polaron hopping process from a $3d$-Mn^{+3} to a $3d$-Mn^{+4} both located in octahedral sites.[4]

High quality of the powder is an important factor in the sensitivity of the thermistors. There are several methods for synthesis of powders, namely the traditional solid solution,[5] ethylene glycol — metal nitrate polymerized complex process,[6] coprecipitation with different precipitators,[7–9] and gel auto — combustion process of nitrate–citrate gels.[10] The results show that the sol–gel combined with the combustion process will lead to a more homogeneous, fine, and highly reactive powder within a shorter time and lower temperature than the traditional process.

The calculation of electronic properties due to the large number of atoms in the unit cell has rarely been studied. Therefore, due to lack of any existing theoretical and experimental results for these compositions, the results of this paper cannot be readily compared with other published results.

In this work, we have synthesized NTC nanopowders with compositions of $NiCo_xMn_{2-x}O_4$ ($x = 0.4, 0.8, 1.2, 1.6$) using the gel auto-combustion method. The average nanopowder size was determined via X-ray diffraction (XRD) and TEM image. The grain size of NTC ceramic is verified with scanning electron microscopy (SEM) images. Fourier transform infrared (FTIR) was employed to confirm the formation of the spinel structure. An *ab initio* calculation of electronic properties of $NiCo_{0.8}Mn_{1.2}O_4$ using full potential of the linear augmented plane wave (FP-LAPW) method was performed. The results indicated that only the $3d$-Mn orbitals play an important role in the conduction mechanism. The dependency of the material resistivity constant (B) and temperature coefficient (α) on the electronic properties of the NTC has been measured.

2. Experimental Procedure

The molar ratio of each chosen composition was based on the formula of $NiCo_xMn_{2-x}O_4$ ($x = 0.4, 0.8, 1.2, 1.6$). Materials used in this experiment were nickel nitrate [$Ni(NO_3)_2 \cdot 6H_2O$], manganese nitrate [$Mn(NO_3)_2 \cdot 4H_2O$], and cobalt nitrate [$Co(NO_3)_2 \cdot 6H_2O$] (Merck, Germany). Aqueous solutions of each single cation were prepared by dissolving each of the raw materials in distilled water. The sol was prepared by mixing the solutions of each cation and then adding the aqueous solution of citric acid to the sol under continuous stirring at 40–50°C and maintaining the pH of 7 by using ammonium hydroxide. The sol was then heated to 70–80°C to evaporate all the water from the remaining gel. The nanopowder was produced by adding nitric acid to the gel, in order to be ignited. The resultant powder was then calcinated at temperatures of 400°C and 750°C. The flowchart for the synthesis of NTC nanopowders is shown in Fig. 1.

3. Results and Discussion

3.1. *Phase analysis and particles size*

The formation of spinel phase has been studied by X-ray diffraction (XRD). Figure 2 shows the XRD diffraction patterns of NTC powders calcinated at 400°C and 750°C for the compounds containing high cobalt concentrations ($NiCo_{1.2}Mn_{0.8}O_4$). These

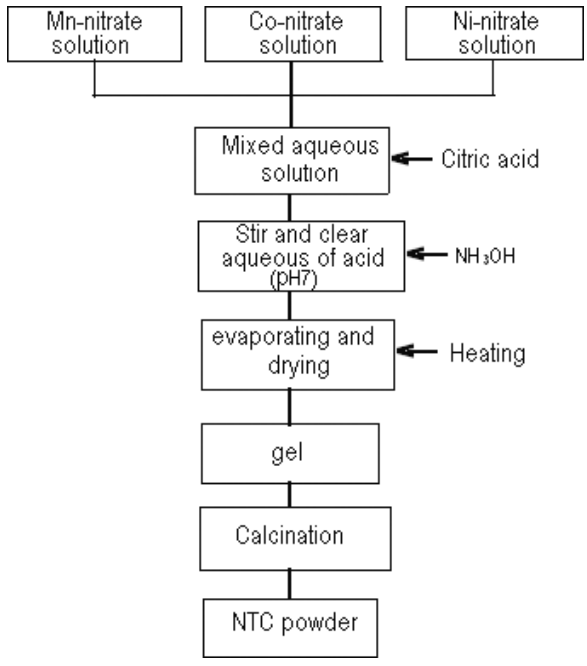

Fig. 1. Flowchart for NTC powder preparation.

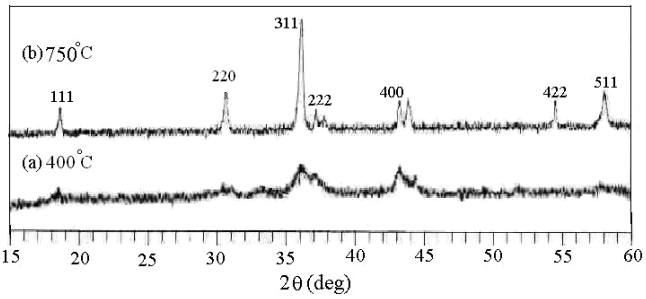

Fig. 2. XRD spectra of the NTC nanopowders calcinated at (a) 400°C and (b) 750°C for the composition of $NiCo_{1.2}Mn_{0.8}O_4$.

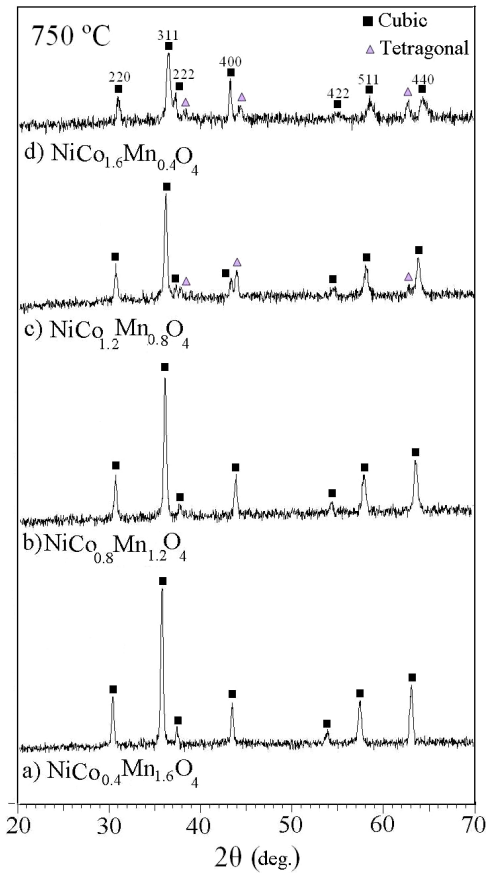

Fig. 3. XRD patterns of four samples of the $NiCo_xMn_{2-x}O_4$ ($x = 0.4, 0.8, 1.2, 1.6$) system.

patterns were obtained using CuK_α radiation in the range of 15−60°. Spinel structure was not formed at low calcination temperature (400°C). However as temperature was increased up to 750°C the spinel structure formation took place. This result seems to be consistent with previously reported results.[11,12] Figure 3 shows the XRD pattern for all compounds starting from low up to high cobalt concentrations.

The compounds at low cobalt concentrations have cubic structure while the samples with high cobalt content have both cubic and tetragonal structure. The calculated results have also indicated that for high cobalt concentration, the lattice parameter decreases and a phase transition occurs. The peak intensity of (311) decreased as the cobalt content increased. However, it seems these samples do not crystallize very well.

The size of particles was determined by means of the X-ray line broadening method using Scherrer's formula: $D = (k\lambda)/(\beta \cos\theta)$, where D is the particle size, λ is the wavelength of the radiation (1.54056 Å for CuK_α radiation), k is a constant equal to 0.94, β is the corrected peak width at half maximum intensity, and θ is the peak position.

The results obtained from Scherrer's formulae for nanopowder size are given in Table 1. In addition, the particle size was determined using transmission electron microscopy (TEM LEO 912B-Germany). The typical TEM image of the particle size for the composition of $NiCo_{1.2}Mn_{0.8}O_4$ calcinated at 750°C and the histogram of particle size are shown in Fig. 4.

The geometric figure of particles is polygonal, and the average particle size obtained from TEM image is about 65 nm, as shown in Fig. 4. Since the size of the particles obtained from the Scherrer equation is bigger than that of the observed one in the TEM image, it can be concluded that Scherrer's relation gives only an approximate value for the particle size.

Figure 5 shows the microstructure of the NTC ceramics sintered at 750°C. The grain size increases

Table 1. NTC nanopowder characteristics prepared by gel auto-combustion calcinated at 750°C.

Composition	Structure	Lattice constant (nm)	Space group	2θ (deg)	Particle size (nm)
$NiCo_{0.4}Mn_{1.6}O_4$	Cubic	$a = 0.8333$	Fd-3m	30.374, 35.764, 63.103	88 (X-ray)
$NiCo_{0.8}Mn_{1.2}O_4$	Cubic	$a = 0.8269$	Fd-3m	30.675, 36.105, 63.606	82 (X-ray)
$NiCo_{1.2}Mn_{0.8}O_4$	Cubic	$a = 8.232$	Fd-3m	30.705, 36.134, 63.892	80 (X-ray) 65 (TEM)
	Tetragonal	$a = 5.835$, $c = 8.423$	I41/amd	37.28, 43.44, 63.88	

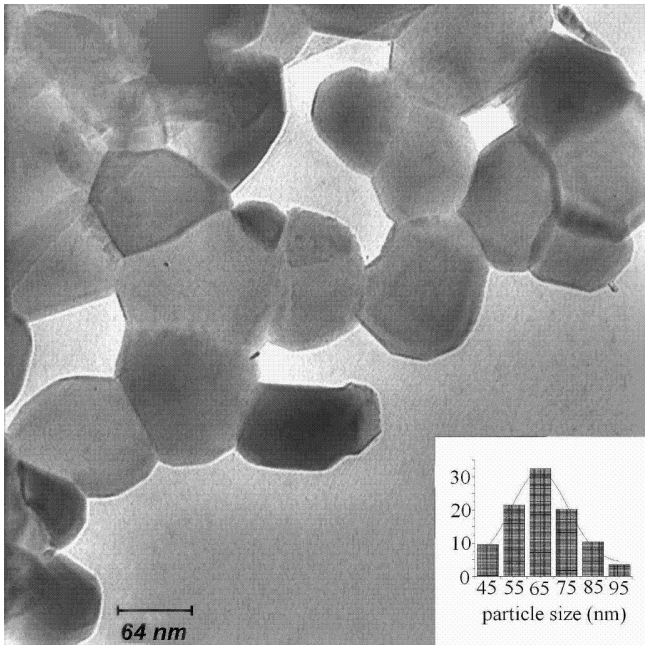

Fig. 4. TEM photograph of the NTC nanopowder for the composition of $NiCo_{1.2}Mn_{0.8}O_4$ calcinated at 750°C.

from about 2 μm up to a few 2 μm with increasing cobalt concentration.

3.2. *FTIR spectrum*

FTIR spectroscopy was used (Shimadzu-4300) to monitor the organic groups and to study the spinel structure. Figure 6 shows the FTIR spectra of the NTC powders in the range of 400−4000 cm^{-1} calcinated at temperature of 750°C for different compounds. In this frequency interval, two broad bands are observed for each spectrum from 400−700 cm^{-1}, which are related to the metal−oxygen bonds (M−O), where M = Ni, Co, Mn. The results are in good agreement with the data published earlier.[6] There are two absorption bands at wavenumbers of about 1480 cm^{-1} and 1590 cm^{-1}, due to C=O stretching vibrations between metal cations and citric acid. The other three peaks are observed at about 2360 cm^{-1}, 2900 cm^{-1}, and 3400 cm^{-1}, which correspond to the variations of CO_2, C−H, and O−H, respectively.[13]

3.3. *Electronic properties*

Calculations have been performed using the full potential linearized augmented plane wave (FP-LAPW) method in the framework of density functional theory (DFT) as implemented in the Wien2k code[14] and in Ref. 15. The Perdew−Burke−Ernzerhof generalized gradient approximation (GGA) was used for the exchange correlation correction.[16,17] The following parameters were chosen for the self-consistency cycles in all computations. The convergence of the basis set is controlled by a cutoff parameter $R_m \times k_{\max} = 7.0$. The value of other parameters are $G_{\max} = 12$ (magnitude of largest vector in charge density Fourier expansion or the plane wave cutoff), $R_{MT}(\mathrm{Ni}) = 2.0$ au, $R_{MT}(\mathrm{Co}) = 2.0$ au, $R_{MT}(\mathrm{Mn}) = 2.0$ au, and $R_{MT}(\mathrm{O}) = 1.6$ au (muffin−tin radius). The iteration was halted when the charge difference dropped to less than 0.001 e between steps as the convergence criterion.

For calculating the electronic properties, a supercell consisting of 80 atoms was used throughout the work. The calculated partial and total density of states (DOS) for $NiCo_{0.8}Mn_{1.2}O_4$ composition are shown in Figs. 7 and 8. The lower and the upper valence bands (VC) mainly consist of 3d-orbitals for Ni, Co, and Mn atoms while for O atom it consist of 2p-O orbitals. The conduction band (CB) for Ni, Co, and Mn atoms also consist of 3d-orbitals and for O atom mainly is 2-p orbit.

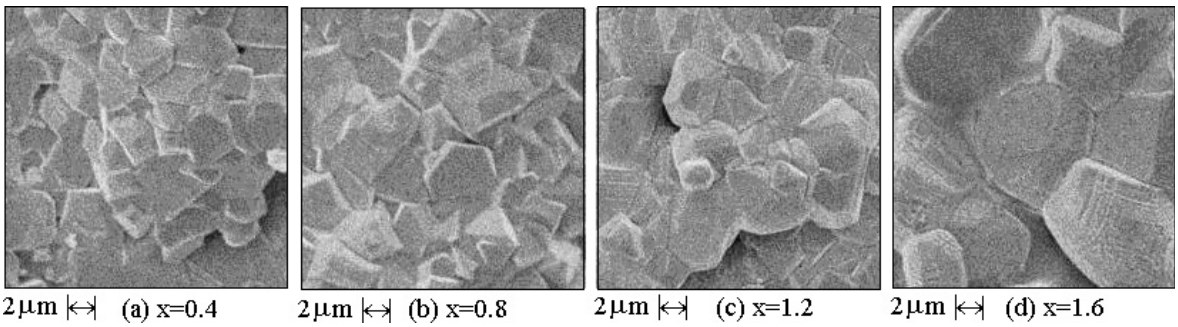

Fig. 5. SEM micrographs of surface of NTC ceramics sintered at 1200°C for $NiCo_xMn_{2-x}O_4$ ($x = 0.4, 0.8, 1.2, 1.6$) system.

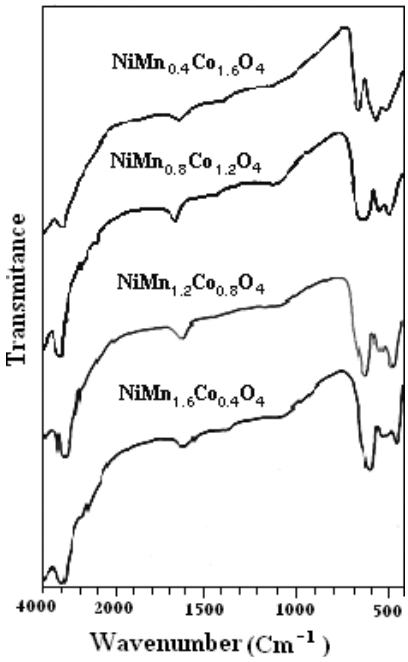

Fig. 6. FTIR spectra of the NTC nanopowders for different compounds calcinated at 750°C.

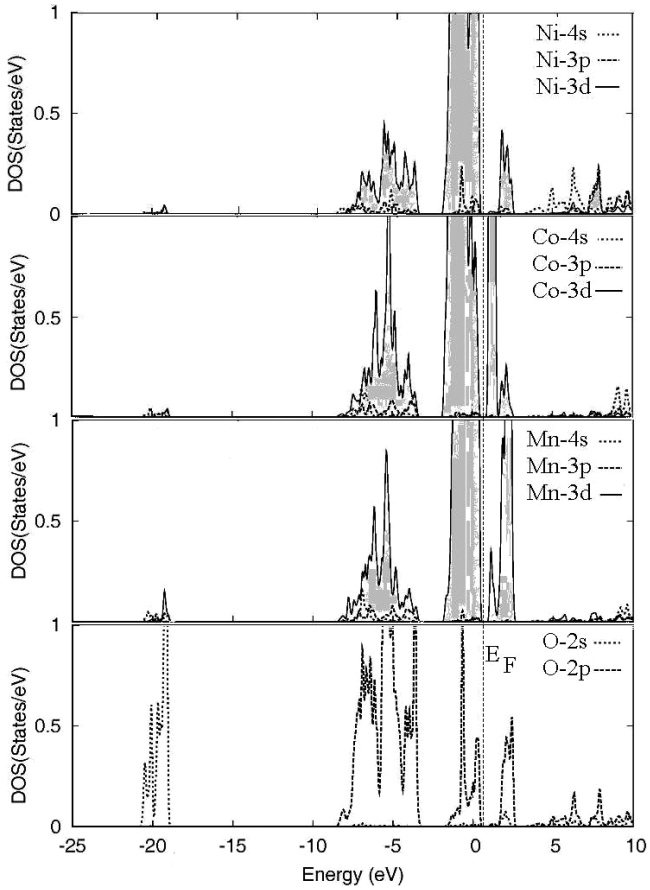

Fig. 7. Partial DOS for $NiCo_{0.8}Mn_{1.2}O_4$ composition.

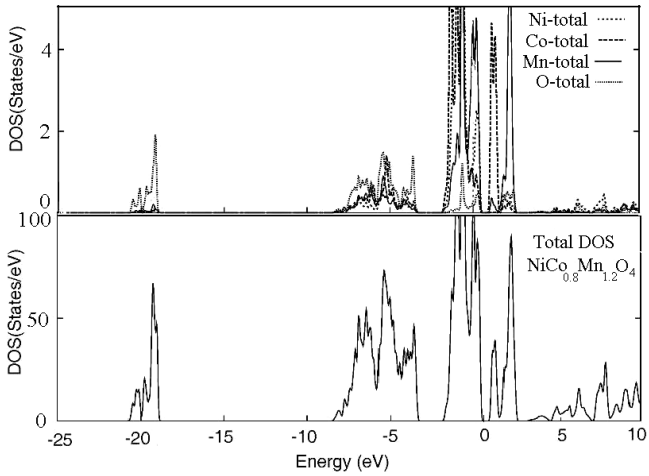

Fig. 8. Total DOS for $NiCo_{0.8}Mn_{1.2}O_4$ composition.

Hybridization of $3d$ orbital for transition metal and $2p$-O orbital are clear from Fig. 7. In fact, the Mn^{+3} in position of an octahedral site is surrounded by four oxygen ions in one plane that attracted the cation and two other oxygen ions above and below plane that pushed away. This lead to split in the five orbitally degenerate $3d$ states of Mn to $e-g$ and $t-2g$ states. Thus, degeneracy of $3d$-Mn provides a basis for polaron hopping process from $3d$-Mn^{+3} to $3d$-Mn^{+4} in octahedral sites.

3.4. *Electrical properties*

The calcinated powder was granulated using PVA as a binder and pressed to form disk-shaped specimens. The specimens were sintered at 1200°C for 4 h in air.

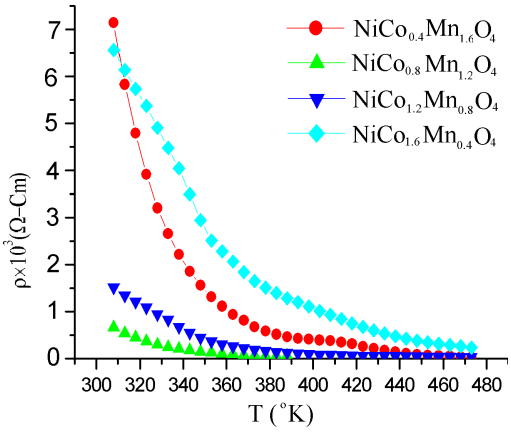

Fig. 9. Variation of resistivity for NTC as function of temperature for the samples prepared by gel auto-combustion process.

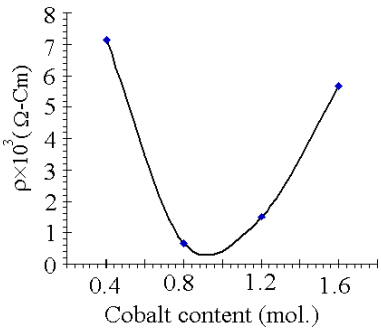

Fig. 10. Variation of DC resistivity of the samples at 308 K perpetrated from nanopowders as function of cobalt content.

The electrical resistance was measured at constant DC voltage and the temperature was measured using a high-resolution (0.1°C) microprocessor-based digital thermometer, model Fluke-51. Figure 9 shows the resistivity-temperature response of gel auto-combustion samples between 308 K and 474 K. The resistivity of the samples at 308 K varies from 665.6 Ω-cm for the sample $NiCo_{0.8}Mn_{1.2}O_4$ to the value of 7140.9 Ω-cm for the sample $NiCo_{0.4}Mn_{1.6}O_4$.

Considering the long-term stability of the sample at low nickel content, the slow diffusion of nickel occurring from one lattice side to another will change the cation distribution and hence the material constant. As these samples have a high nickel content, most lattice sites will be saturated and a very small amount of nickel atoms may also diffuse causing the system to become more stable.[18]

Figure 10 shows the values of the DC resistivity of the samples, prepared by gel auto-combustion process, as function of cobalt content at 308 K. DC resistivity of the sample for $x = 0.4$ is the highest and decreases with increasing cobalt content. For $x = 0.8$, the resistivity is minimum and increases by increasing the amount of cobalt in the samples.

The material constant, B, and the temperature coefficient, α, have been evaluated as follows[5]:

$$B = \ln \frac{(\rho_1/\rho_2)}{(1/T_1 - 1/T_2)}\,, \tag{1}$$

$$\alpha = (-B)/T^2\,, \tag{2}$$

where ρ_1 and ρ_2 are the nominal values of resistivity at T_1 and T_2, respectively.

Since the electrical properties of NTC depend much on the grain size, using nanopowder to prepare NTC samples results in small grain sizes at short sintering time and hence different electrical properties.

Figure 11 shows the Arrhenius plot of the resistivity of the composites in the low-temperature range. It can be seen clearly that the composites exhibited almost the same temperature dependence as the single-phase spinel oxide.

The measured values of B and α for different compositions are summarized in Table 2. The results indicate that the maximum value of B occurs when the content of cobalt is about $x = 0.4$. Furthermore, the electrical properties of NTC also

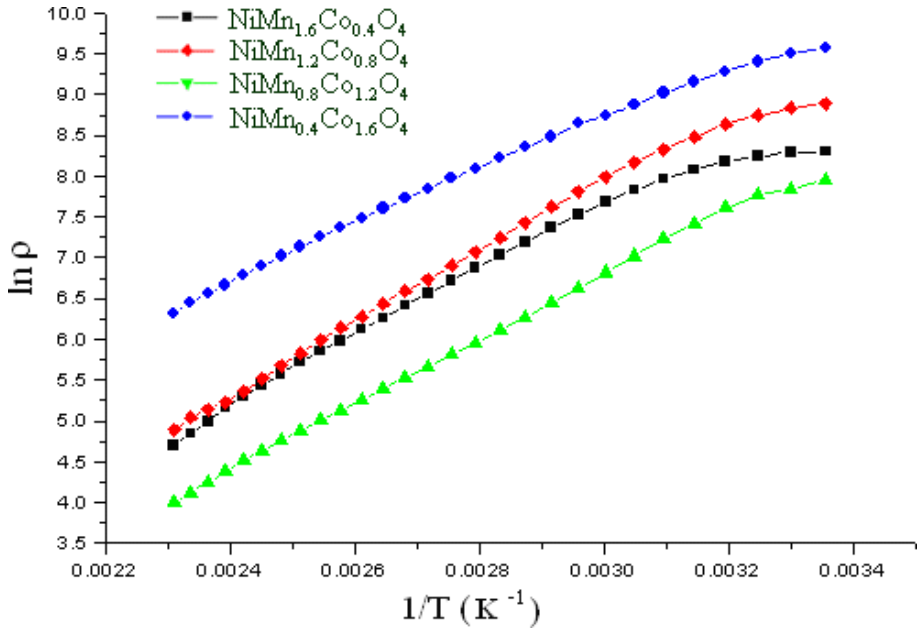

Fig. 11. Arrhenius plot of resistivity for $NiCo_xMn_{2-x}O_4$ ($x = 0.4, 0.8, 1.2, 1.6$) system.

Table 2. Electrical parameters of NTC prepared by gel auto-combustion.

Sintering temperature and time	Composition	B (K)	α [25°C] (K^{-1})	Preparation method	Structure
This work					
1200°C, 4h	$NiCo_{0.4}Mn_{1.6}O_4$	4283	−4.82	Gel auto-combustion	Cubic
1200°C, 4h	$NiCo_{0.8}Mn_{1.2}O_4$	3620	−4.07	Gel auto-combustion	Cubic
1200°C, 4h	$NiCo_{1.2}Mn_{0.8}O_4$	3455	−3.89	Gel auto-combustion	Cubic + Tetragonal
1200°C, 4h	$NiCo_{1.6}Mn_{0.4}O_4$	2851	−3.22	Gel auto-combustion	Cubic + Tetragonal
Others					
1250°C, 6h[18]	$NiCoMnO_4$	3649	−4.15	Mixed Oxide	—
1200°C, 2h[19]	$NiCoMnO_4$	3515−3940	—	Coprecipitation process	—
1400°C, 3h[20]	$Mn_{(1.75-1.25X)}Co_{2.5X}Ni_{1.25(1-X)}O_4$ $(0 \leq X \leq 0.6)$	3400−4100	—	Mixing Mn, Co, and Ni nitrates	Cubic
1150°C −[10]	$Ni_1Co_{0.2}Mn_{1.8}O_4$	3360−3350	—	Gel auto-combustion (nitrate−citrate gels)	Cubic
−, −[21]	Mn:Co:Ni (45.0:29:26)	3280		Mixed oxide (thick film)	—

depend strongly on the grain size.[5] Therefore, one expects that the samples made from nanopowders will have smaller grain size and hence smaller value of B if the sintering time chosen was very short. However, increasing the sintering time will result in larger grain size and hence improved electrical parameters.

4. Conclusions

Mn, Co, and Ni ternary oxide nanopowders having spinel structure, which can be used as NTC thermistors, were prepared by gel auto-combustion method. XRD results show that the spinel structure is formed at 750°C. The spinel structure starts forming at 400°C and by increasing the temperature to 750°C the percentage of spinel phase continuously increases and seems to be completed at 750°C. This is also confirmed by FTIR spectra. The average particle size which was determined using both TEM image and Scherrer's formulae was found to be about 65−80 nm.

Ab initio calculation indicated that the lower and upper valence band mainly consists of 3*d*-orbitals for Ni, Co, and Mn atoms while for O atom it consists of 2*p*-O orbitals. The conduction band for Ni, Co, and Mn atoms also consists of 3*d*-orbitals and for O atom it is mainly 2*p*-orbital. There is a hybridization between 3*d* orbital of these metals and 2*p*-O orbital. The degeneracy of 3*d*-Mn provides a basis for polaron hopping process from 3*d*-Mn^{+3} to 3*d*-Mn^{+4} in octahedral sites.

The dependence of material resistivity constants (B) and temperature coefficient (α) have been measured and the results for the different samples were compared.

References

1. R. C. Buchanan (ed.), *Ceramics Materials for Electronics — Processing, Properties and Application* (Marcel Dekker Inc., 1991).
2. A. J. Moulson and J. M. Herbert, *Electroceramics Materials, Properties, Applications*, 2nd edn. (John Wiley & Sons Ltd., 2003).
3. R. Schmidt, A. Basu and A. W. Brinkman, *Phys. Rev. B* **72**, 115101 (2005).
4. S. Fritsch, J. Sarrias, M. Brieu, J. J. Couderc, J. L. Baudour, E. Snoeck and A. Rousset, *Solid State Ionics* **109**, 229 (1998).
5. M. Hosseini and B. Yasaei, *Ceram. Int.* **24**, 543 (1998).
6. P. Duran, J. Tartaj, F. Rubio, C. Moure and O. Pena, *J. Eur. Ceram. Soc.* **24**, 3035 (2004).
7. J. L. Martin De Vidales, *J. Mater. Sci.* **33**, 1491 (1998).
8. R. Schmit, A. Stiegelschmitt, A. Roosen and A. W. Brinkman, *J. Eur. Ceram. Soc.* **23**, 1549 (2003).
9. A. Díez, R. Schmidt', A. E. Sagua, M. A. Frechero, E. Matesanz, C. Leon and E. Morán, *J. Eur. Ceram. Soc.* **30**, 2617 (2010).
10. W. Wang, X. Liu, F. Gao and Ch. Tian, *Ceram. Int.* **33**, 459 (2007).
11. Y. Abe, T. Meguro, S. Oyamatsu, T. Yokoyama and K. Komeya, *J. Mater. Sci.* **34**, 4639 (1999).
12. T. Yokoyama, T. Meguro, Y. Shimada, J. Tatami, K. Komeya and Y. Abe, *J. Mater. Sci.* **42**, 5860 (2007).

13. K. Nakamoto, *Infrared and Raman Spectra of Inorganic and Coordination Compounds* (John Wiley & Sons, 1997).
14. P. Blaha, D. Singh, P. I. Sorantin and K. Schwarz, *Phys. Rev. B* **46**, 1321 (1992).
15. J. P. Perdew, J. A. Chevary, S. H. Vosko, K. A. Jackson, M. R. Pederson, D. J. Singh and C. Fiolhais, *Phys. Rev. B* **46**, 6671 (1992).
16. M. Peterson, F. Wanger, L. Hufnagel, M. Scheffler, P. Blaha and K. Schwarz, *Comput. Phys. Commun.* **126**, 294 (2000).
17. P. Blaha and K. Schwarz, WIEN2k, http://www.wien2k.at/, Vienna University of Technology, Austria (2002).
18. M. Hossein, *Ceram. Int.* **26**, 245 (2000).
19. J. Zhuang, A. Chang, Zh. Jia, Sh. Zhuang and D. Jia, *Ceram. Int.* **30**, 1661 (2004).
20. T. Yokoyama, T. Meguro, M. Nakamura, J. Tatami, T. Wakihara and K. Komeya, *J. Ceram. Process. Res.* **10**, 683 (2009).
21. J. Huang, Y. Hao, H. Lin, D. Zhang, J. Song and D. Zhou, *Mater. Sci. Eng. B* **99**, 523 (2003).